

# COSMOSOMAS Observations of the CMB and Galactic Foregrounds at 11 GHz: Evidence for anomalous microwave emission at high Galactic Latitude.

S. R. Hildebrandt<sup>1</sup>, R. Rebolo<sup>1,2</sup>, J. A. Rubiño-Martín,<sup>1</sup> R. A. Watson<sup>1,3</sup>,  
C. M. Gutiérrez<sup>1</sup>, R. J. Hoyland<sup>1</sup> and E. S. Battistelli<sup>1,\*</sup>

<sup>1</sup>*Instituto de Astrofísica de Canarias, 38200 La Laguna, Tenerife, Spain.*

<sup>2</sup>*Consejo Superior de Investigaciones Científicas, Spain.*

<sup>3</sup>*Jodrell Bank Observatory, University of Manchester, Macclesfield, Cheshire SK11 9DL, UK.*

\* *Present address: University of British Columbia Department of Physics and Astronomy, 6224 Agricultural Road Vancouver, B.C. Canada V6T 1Z1.*

Accepted —; received —; in original form 12 November 2021

## ABSTRACT

We present observations with the new 11 GHz radiometer of the COSMOSOMAS experiment at the Teide Observatory (Tenerife). The sky region between  $0^\circ \leq RA \leq 360^\circ$  and  $26^\circ \leq DEC \leq 49^\circ$  (ca. 6500 square degrees) was observed with an angular resolution of  $0.9^\circ$ . Two orthogonal independent channels in the receiving system measured total power signals from linear polarizations with a 2 GHz bandwidth. Maps with an average sensitivity of  $50 \mu\text{K}$  per beam have been obtained for each channel. At high Galactic latitude ( $|b| > 30^\circ$ ) the 11 GHz data are found to contain the expected cosmic microwave background as well as extragalactic radiosources, galactic synchrotron and free-free emission, and a dust-correlated component which is very likely of galactic origin. At the angular scales allowed by the window function of the experiment, the dust-correlated component presents an amplitude  $\Delta T \sim 9\text{--}13 \mu\text{K}$  while the CMB signal is of order  $27 \mu\text{K}$ . The spectral behaviour of the dust-correlated signal is examined in the light of previous COSMOSOMAS data at 13–17 GHz and WMAP data at 22–94 GHz in the same sky region. We detect a flattening in the spectral index of this signal below 20 GHz which rules out synchrotron radiation as being responsible for the emission. This anomalous dust emission can be described by a combination of free-free emission and spinning dust models with a flux density peaking around 20 GHz.

**Key words:** cosmology: observations – cosmic microwave background – Galactic anomalous emission – Galactic foregrounds

## 1 INTRODUCTION

Since 1984, the Teide Observatory has hosted experiments to observe the cosmic microwave background at 10–33 GHz on angular scales from degrees to arcminutes. Located at this observatory, the COSMOSOMAS experiment consists of two radiotelescopes designed to acquire sensitive observations of the microwave sky at frequencies in the range 10–17 GHz with an angular resolution of  $\sim 1$  degree. It was conceived as a high resolution extension of the Tenerife experiment (Davies et al. 1996; Hancock et al. 1997; Gutiérrez et al. 2000) with the goal to provide 10–17 GHz ground-based data of angular resolution comparable to the lowest frequency channel of the Wilkinson Microwave Anisotropy Probe, WMAP (Bennet et al. 2003a). Observations in this frequency range can contribute significantly to a better understanding of the foreground emission and to improve the limits imposed on cosmo-

logical parameters by present and future CMB experiments. This appears particularly relevant for missions like Planck<sup>1</sup> which are planned to achieve a sensitivity of order  $1 \mu\text{K}$  per resolution element and infer cosmological parameters with accuracy better than 1%.

There is also an increasing interest in sky maps at few tens of GHz to elucidate the presence of a new microwave emission process different to the three classical Galactic foregrounds, namely, synchrotron, free-free and thermal dust emission. First detected as a dust-correlated signal in the COBE/DMR data (Kogut et al. 1996), this microwave emission was initially interpreted as due to free-free radiation. However, statistical detections of dust correlated signals by experiments like CBI

<sup>1</sup> <http://www.rssd.esa.int/index.php?project=PLANCK>

(Mason et al. 2001), Saaskaton (de Oliveira-Costa et al. 1997), OVRO (Leitch et al. 1997), the Tenerife experiment (de Oliveira-Costa et al. 1999; de Oliveira-Costa et al. 2004) and also in the Green Bank Galactic Plane Survey (4.85 GHz) (Finkbeiner et al. 2004) strongly suggested that free-free emission cannot be the only underlying process. Draine and Lazarian (1998a,b) alternatively proposed electric dipole radiation from spinning particles and magnetic dipole emission as mechanisms behind this anomalous microwave emission.

A dust correlated signal has also been detected in the WMAP data (Lagache 2003, Bennet et al. 2003a) but its interpretation is still a matter of debate. Bennet et al. 2003a argue that all foreground emission observed at WMAP frequencies can be explained in terms of the three classical foreground components. However, de Oliveira-Costa et al. (2004) show that the synchrotron template at 22 GHz derived by the WMAP team under the previous assumption correlates with the 10 and 15 GHz Tenerife data in a manner incompatible with the frequency behaviour of synchrotron emission. More recently, Fernández-Cerezo et al. (2006) using high Galactic latitude observations at 13-17 GHz obtained with the first radiometer (COSMO15) of the COSMOSOMAS experiment (over an area of more than 3000 deg<sup>2</sup>) find evidence that below 20 GHz the spectrum of the dust correlated signal turns over just as predicted by spinning dust emission. Unambiguous evidence for anomalous microwave emission in individual astronomical objects has been found by the COSMOSOMAS experiment (Watson et al. 2005) in the Perseus molecular complex and by CBI in the dark cloud LDN1622 (Casassus et al. 2006).

In this paper, we present new results of the COSMOSOMAS experiment<sup>2</sup> obtained with the 11 GHz radiometer, hereafter referred as COSMO11. These observations cover a sky region of 6500 deg<sup>2</sup> with an angular resolution of  $\sim 1^\circ$  and sufficient sensitivity to explore further the behaviour of the anomalous microwave emission and other foregrounds at high Galactic latitudes. While we find cosmic microwave background and extragalactic radiosources dominate the temperature fluctuations at 11 GHz in our beam scale, we also detect a highly significant dust-correlated signal at this frequency which is compared with previous results in the same region using COSMO15 and WMAP data.

## 2 THE COSMO11 RADIOMETER

The COSMOSOMAS experiment consists of two independent similar radiotelescopes (COSMO15 and COSMO11) aimed to obtain measurements of the microwave radiation in the frequency range 10-17 GHz with average resolution of  $0.9^\circ$  (FWHM). The experiment is sited at Teide Observatory (2400m altitude, Tenerife) and details of the observational strategy can be found in (Gallegos et al. 2001). Essentially, each of the two instruments performs daily observations of a strip in the sky with diameter  $20^\circ$  in DEC, centred at the meridian. Earth rotation produces a map with complete RA coverage. An area equivalent to  $\sim 14\%$  of the whole sky is then covered daily with a typical sensitivity of 1.0–2.0 mK per pixel, or roughly 0.3–0.7 mK per beam, after removal of most atmospheric contamination (see Sect. 3.1).

COSMO11 started scientific operation at the end of 2003, several years later than the higher frequency COSMO15, however its

**Table 1.** Summary of geometric configurations and observed declinations (complete in RA) in this work. Tilt has always been  $5^\circ$ . Units in degrees.

Period	$\alpha$	$\beta$	DEC <sub>min</sub>	DEC <sub>max</sub>
01/11/03-12/05/04	26.00	64.50	30.80	50.80
23/05/04-10/06/05	29.50	64.50	23.80	43.80

good overall performance has resulted in similar sensitivities to COSMO15 in a much shorter time scale. In this work, we present COSMO11 and analyze data taken from November 2003 to 10<sup>th</sup> June 2005. By stacking the best first 150 good observing days, COSMO11 achieves a comparable sensitivity, 40–50  $\mu$ K per beam, to that of COSMO15 data (Fernández-Cerezo et al. 2006).

The COSMO11 radiometer was equipped with two similar receivers, working at almost identical frequencies, but sensitive to orthogonal polarizations in order to provide a better control of systematics and explore potential polarization measurements.

### 2.1 Experimental layout

The optical and mechanical structure of the COSMO11 experiment (see Fig. 1) is very similar to that of COSMO15. The main differences are the size of the circular, primary, flat, mirror of 3.0 m (instead of 2.5 m) and the aperture of the parabolic, secondary, mirror which is 2.4 m instead of 1.8 m. Both instruments were designed to achieve an angular resolution of  $0.9^\circ$ . A metal block with a  $5^\circ$  opening angle tilts the main, flat mirror. In this way as the mirror spins (at  $\sim 1$  Hz), the observed path in the sky describes a circle of  $20^\circ$  of diameter. During the period of observations relevant to this paper the inclination of the primary mirror has been changed twice while the position of the parabolic dish and the tilt of the primary mirror were kept fixed. A change of the inclination of the primary mirror causes a displacement in DEC of the center of the ring described by the beam on the sky. In Tab. 1 we give a summary of the values for the main geometrical parameters. The setup adopted for the observations led to data acquisition from declination  $23.80^\circ$  to  $50.80^\circ$ .

### 2.2 Receivers

The COSMO11 receiver is a polarimeter, designed to receive orthogonal linear polarisations through 2 total power channels (see Fig. 2).

The whole front-end of the receiver is housed in a cryostat and cooled to 15-20K by a dual-staged helium gas refrigerator. The phase centre of the feedhorn coincides with the focal plane of the offset parabola. This provides the alignment of the cryostat. The cryostat window is a sandwich of thin Mylar film and high density polypropylene foam. Secondary calibration is provided by a temperature controlled broadband noise source which enters the beam through a side lobe. This coupling is obtained by placing the calibration probe close to the cryostat window but not in the main beam. The feed horn is a conical corrugated design for maximum efficiency and minimum side lobes. The feed horn is followed by an orthomode junction. Both are designed by ERA technology Ltd and are matched to the Channel master 2.4m offset parabolic antenna. The two linear polar channels feed two similar 10-12GHz cryogenically cooled amplifiers from Berkshire Technologies Inc. The noise temperatures are close to 10K and the gain is 25dB minimum. The complete total power channels form direct detection

<sup>2</sup> <http://www.iac.es/project/cmb/cosmosomas> of the Instituto de Astrofísica de Canarias.

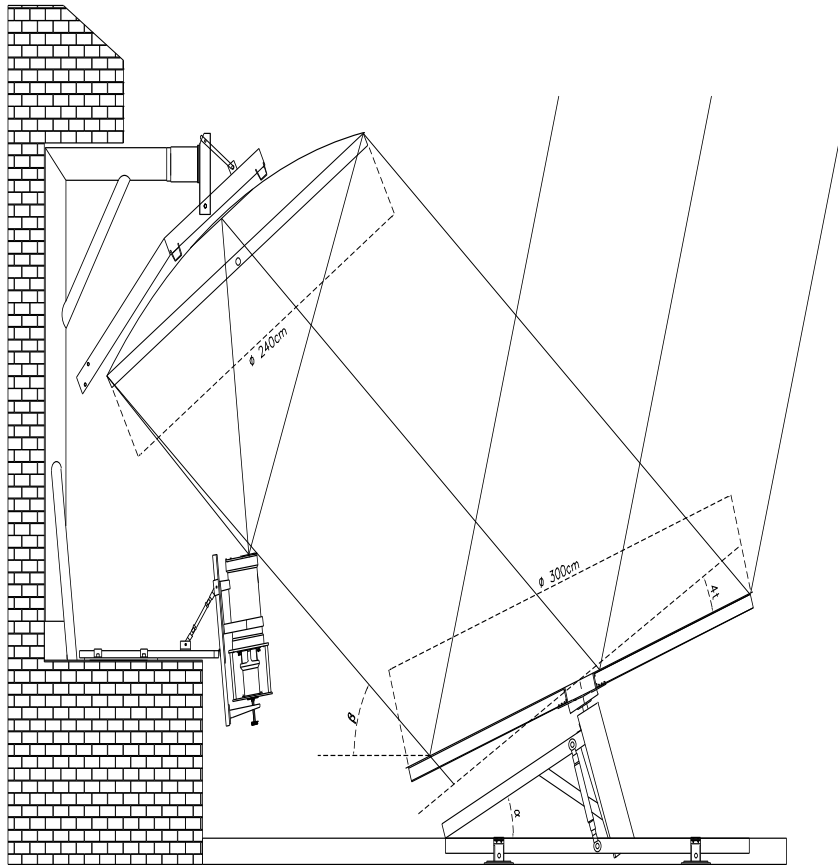


Figure 1. Optical system and mechanical structure of COSMO11.

chains whereby a matched square-law detector is used to detect the microwave signal without first mixing the signal down to an intermediate frequency. The receiver response just before entering the detectors is shown in Fig. 3. The mean, weighted, frequency defined as:

$$\bar{\nu} := \int_{\nu_{min}}^{\nu_{max}} \nu \rho(\nu) d\nu, \quad (1)$$

where  $\rho(\nu)$  is the normalized (by setting its integral to unity) linear spectral response of the filters, yields 10.89 GHz for channel 1 and 10.87 GHz for channel 2. The overall  $1/f$  knee frequency is about 3Hz, which is faster than the spinning flat plate frequency of 1Hz. The  $1/f$  is removed from the data stream by eliminating sufficient Fourier harmonics. See section 2.3. The rest of the receiving system is analogous to that of COSMO15 (Fernández-Cerezo et al. 2006).

### 2.3 Receiver orientation and scanning strategy

In this work, we only deal with data obtained for the primary configuration with channel 1 and 2 polarizations oriented North-South and East-West, respectively, see Tab. 2. In order to perform polarization studies, it is necessary to rotate the receiver system and take data with a second orientation, e.g., with a  $45^\circ$  relative rotation with respect to the primary configuration. Observations in this second configuration are being currently conducted and polarization measurements of the Galactic foregrounds and the cosmic microwave background will be considered in a future paper,

Table 2. Summary of the receiver configurations. The orientations referred to local meridian. Useful days are also given for Channel 1 and 2, respectively.

Period	Channel 1	Channel 2	Useful days
01/11/03-10/06/05	North-South	East-West	135, 140

although a faint polarized emission has been already measured in the Perseus molecular complex with the first data obtained so far (Battistelli et al. 2006).

In order to minimize the effect of systematics in the data set, we also rotated the cryostat by  $90^\circ$ , which essentially produces an exchange in the receivers of channel 1 and 2.

In Fig. 18, the scanning strategy of COSMO11 is shown. The circles in RA and DEC, the sky coverage due to Earth rotation, and the two polarizations, pointing towards the Celestial north pole: one North-South; the other, East-West. Since we are also interested in Galactic foreground emission, we also give a figure of the scanning strategy in Galactic coordinates. The sky image is that of the lowest frequency WMAP channel, i.e. K band. One can readily see the crossing of COSMOSOMAS rings with the Galactic plane, both center and anti center regions, and the high Galactic latitude region observed. We also note the position of Cygnus A, our main calibrator.

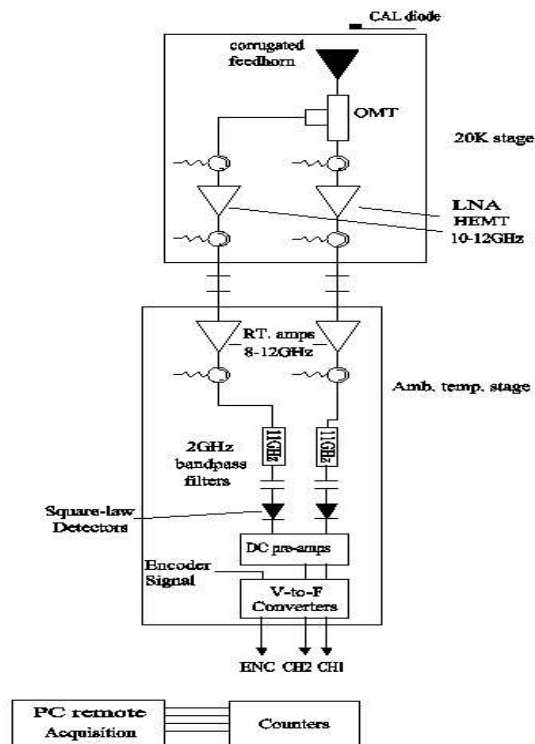


**Figure 2.** Receiver system of COSMO11. Two polarizations of total power signal at  $\sim 10.9$  GHz are observed.

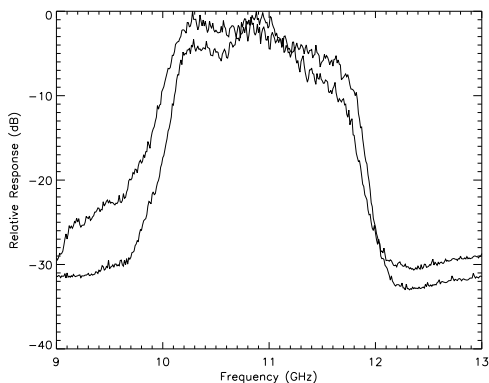


**Figure 3.** Relative spectral responses of the two filter band passes in COSMO11.

## 2.4 Data acquisition

The COSMO11 data acquisition procedures are similar to those used in COSMO15. Data are sampled over  $4000 \mu\text{s}$ , leaving a blanking time of order  $400 \mu\text{s}$ . A Fast Fourier Transformation is applied to the data for each mirror cycle, keeping 106 harmonics. In practice, we find that for the construction of the daily maps, it is enough to consider up to the 45<sup>th</sup> harmonic; higher harmonics do not contain astronomical information. Then, the data gathered every  $\sim 30\text{s}$  are stacked together, yielding a mean value for each of the 106 harmonics and their corresponding standard deviations.

We note that in 30 s the apparent motion of the sky corresponds to  $\sim 0.12^\circ$ . Since the beam size is around  $0.9^\circ$ , there is no problem in averaging data every  $\sim 30$  s. This is done mainly to save memory and allow faster data processing. Nevertheless, we store independently the data obtained for each spin of the mirror every  $\sim 1$  s mainly for the technical monitoring of the data acquisition system. Every second, a diode signal of 2 K is introduced in the feed horn. This allows to measure changes in the receiver gain. Each day of data is saved into a FITS binary file.

Every 30 s a stacked data set, called here a *scan* is stored. Each scan is comprised of 275 samples. In this way, each sample corresponds to an angular size of order  $\pi D/275$ , where  $D$  is the diameter of the circle subtended by the COSMO11 beam on the sky. From Sect. 2.1,  $D$  is  $\sim 20^\circ$  and therefore the angular size of each sampling index is  $\sim 0.23^\circ$ . Summarizing, the angular size of the data bin is of order  $0.12^\circ \times 0.23^\circ$ , which is appropriate for the beam angular resolution of COSMO11 (eventually, for the astronomical map we will choose a pixelization of  $1/3^\circ \times 1/3^\circ$ ).

## 3 DATA PROCESSING

In this section, we describe the data analysis of COSMO11 observations, from the daily map making procedure and calibration to the cumulative maps corresponding to a period of approximately 110 equivalent observing days for each channel.

### 3.1 Daily processing

The first step is the correction of gain fluctuations in the data. To that end, we divide the counts measured in each scan by the value of the 2 K calibration diode corresponding to that scan. A first clipping of bad data is performed on the scans consisting of rejection of those with saturated signals, no signal, spikes and/or glitches. The result is a sequence of scans with total power signal in acceptable ranges.

In addition to instrumental noise, our data are affected by atmospheric emission which causes a modulation in the total power every spin of the primary mirror (see Fig. 4). After probing some techniques to remove this atmospheric modulation, we arrived to the conclusion that subtraction of a Fourier fit to *each* scan is a suitable and efficient procedure. In this way, we also remove the main part of  $1/f$ -like noise. At 11 GHz, it suffices to remove some low order Fourier terms in order to get useful data (see later, Fig. 10). However, for the sake of a direct comparison with the previous COSMO15 data, notably more affected by atmospheric emission than the current experiment, we choose here the same number of Fourier terms to be removed in each scan, i.e., a Fourier series fit of 7<sup>th</sup> order (i.e., a constant term plus seven sin and cos terms). The fit of any scan is thus independent from the rest. In the Fourier series fit to each scan, we mask any single data sample within a radius of  $0.4^\circ$  of a signal exceeding 4 times the standard deviation of the scan data. This is done to minimize the effect of bright sources on the fitted curve. After this individual scan cleaning a second clipping is applied consisting of rejection of scans with standard deviation 20 times larger than the mean standard deviation of the three preceding and three following scans.

After this processing has been executed, we still find a much weaker daily modulation of the data taken at the same sky position (same line of sight or same sample index). This modulation is possibly associated to day-night atmospheric temperature variations. We correct it removing the first four Fourier terms in the fit to the

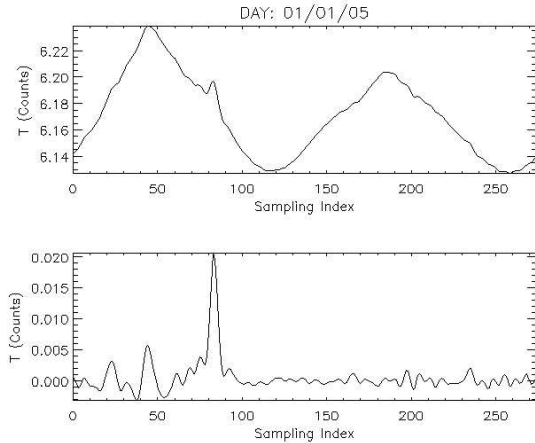


**Figure 4.** Typical scan obtained with COSMO11. Up: atmospheric emission appears clearly as a long-scale modulation. The peak close to sampling index 85 corresponds to the observation of the Cygnus A region. Down: total power after subtraction of the first seven Fourier harmonics. Structures to the left side of the Cygnus A region are associated to nearby galactic plane regions.

whole day-night data set in any sky position. Here again, data in a  $0.4^\circ$  interval centred in points which exceed the day-night mean value in  $4\sigma$  are masked in the Fourier series fit. The correction applied to the day-night modulation modifies the window function of the experiment (?). Because of the masking of the bright sources during the fitting procedure applied to the day-night modulation, the effect on point sources is very small, however CMB, very weak sources and diffuse foregrounds are affected and will be taken into account when generating adequate templates for cross-correlation with the experiment data.

### 3.1.1 Daily map making

Due to the scanning strategy of COSMO11, each astronomical source is observed twice (except in the upper and bottom sections of the scan). Fig. 5 shows the sequence of scans divided into its 275 sampling sections (vertical axis) in terms of the scan number (time). The two point-like sources placed at approximately (2150,12) and (2250,85) correspond to the first and second crossing of Cygnus A with the beam of the experiment. Other sources are also seen daily, but with insufficient signal/noise ratio to be used as primary calibrators. For example, GB6 0319+4130 (3C84) can be seen at around (200,270). This source is known to show variability. From the 1980s until the epoch of the COSMOSOMAS observations, its flux has decreased from  $\sim 50$  Jy to  $\sim 20$  Jy. Our observations are in agreement with the flux extrapolated from the WMAP K band measurement ( $S = 11.1 \pm 0.1$  Jy) and the spectral index published for this source by the WMAP team ( $\alpha = -0.8 \pm 0.1$ ). The other bright sources seen in the map are complex structures in the Galactic plane towards the anti center.

This double measurement of any sky region is then used in the construction of a daily map. First, knowing the local time of the entrance and exit of a known point-like source, say Cygnus A, we compute their hour angle (HA). Next, we use the values of the declination of the source and also the direct measure of the inclination of the main, flat, mirror ( $\alpha$ ) and of the tilt angle ( $\theta$ ) as starting values to compute optimal values for the geometrical parameters that make to coincide the derived and observed HA.

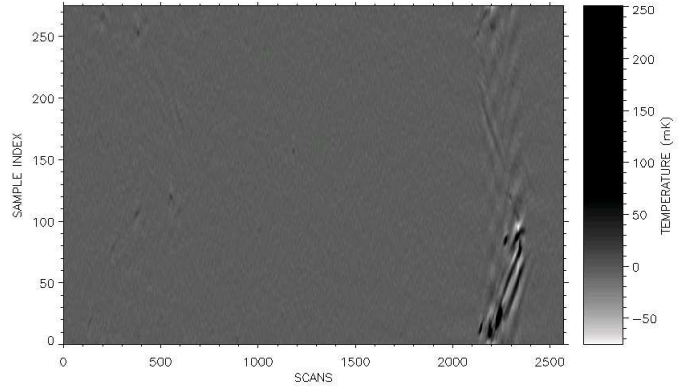


**Figure 5.** Scan sequence for a typical day in the COSMO11 data. Scans are cleaned. Notice the duplication of the observed sky region. The Galactic Cygnus region and Cygnus A are clearly observed near scan number 2000. The brightest sources seen along the first scans are the complex regions towards the Galactic anti-center.

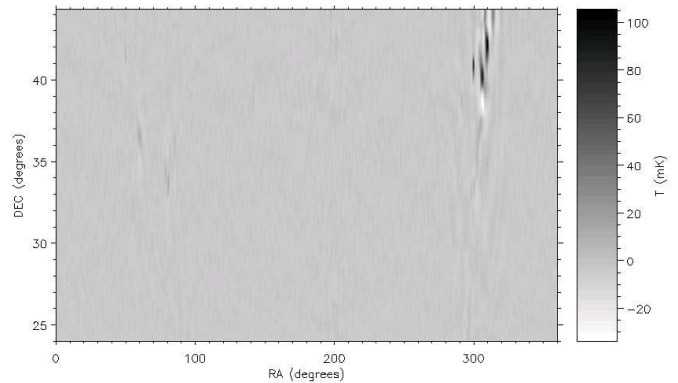


**Figure 6.** Typical daily map. The Galactic Plane crossing is clearly seen, including the Cygnus A complex. Also clearly detected is the crossing towards the anti center region.

Once,  $\alpha$ ,  $\beta$  and  $\theta$  are inferred, we construct a daily map by projecting each of the observed pixels into a rectangular grid with RA in its horizontal axis and DEC in its vertical one (see Fig. 6). The chosen pixelization is  $1/3^\circ \times 1/3^\circ$ , which is adequate for the angular size of the sampling index and for the size of the beam. Due to the range of observed declination ( $20^\circ$ ), this method is appropriate and we do not resort here to more refined methods as the Healpix pixelization.

### 3.1.2 Daily flux/temperature calibration

Each daily set of data is calibrated in flux or antenna temperature with observations of the brightest stable point-like radio source in our maps: Cygnus A (see Fig. 6). In Fig. 7 one of the daily images of Cygnus A observed by COSMO11 is plotted.

We use the empirical model by (Baars et al. 1977) to derive the expected flux density ( $S$ ) from Cygnus A. For our frequency range it gives

$$\log S_{\text{Cyg}}^B [\text{Jy}] = a + b \log \nu [\text{MHz}], \quad (2)$$

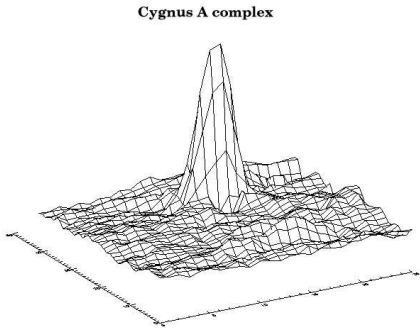


**Figure 7.** Cygnus A as recorded in a *single day of observation* by COSMO11.

where  $a = 7.161 \pm 0.053$  and  $b = -1.244 \pm 0.014$  which leads to a flux of Cygnus A of  $S_{\text{Cyg}}(10 - 12\text{GHz}) = 153 - 122\text{Jy}$ .

For each daily observation of Cygnus A we check the beam of the instrument by fitting a two-dimensional Gaussian with an allowed base-label offset. In the frequency range of COSMO11, the Rayleigh-Jeans limit applies. Therefore, the antenna temperature associated with a given flux from Cygnus A is

$$T(\nu) = \frac{c^2}{2k} \frac{S_{\text{Cyg}}(\nu)}{\nu^2 \Omega}, \quad (3)$$

where  $c$  is the vacuum speed of light,  $k$  is the Boltzmann's constant and  $\Omega = (\pi/4 \ln 2) \text{FWHM}^2$  is the solid angle subtended by the beam.

The effect of the band-pass filters is to yield a weighted antenna temperature for each observation of Cygnus A according to

$$T_{\text{CygA}}^C = \int_{\nu_{\min}}^{\nu_{\max}} \rho^C(\nu) T_{\text{CygA}}^B(\nu) d\nu, \quad (4)$$

where the script  $C$  stands for channel and  $T_{\text{Cyg}}^B$  is simply Eq. 3 with  $S$  replaced by Eq. 2 and where  $\rho^C(\nu)$  is the normalized linear spectral response of each filter. Assuming a circular FWHM of  $1^\circ$  the antenna temperature results 110.2 mK and 110.9 mK for channel 1 and 2, respectively. For the fluxes, we get 137.9 Jy and 138.3 Jy for channel 1 and 2, respectively. This shows that the differences due to non identical band-pass filters are of order  $\sim 0.5\%$  only. In Sect. 3.2 we plot the distribution of daily root mean square (RMS) in clean regions.

On the other hand, for a beam size of  $1^\circ$ , the polarization of the Cygnus A region is less than 3-5%. We have not attempted to perform a detail study of the expected difference of the calibration for each of the two channels taking into account the COSMOSOMAS scanning strategy and data processing. The reason is that, as explained later, the cumulative maps of each channel are recalibrated against unpolarized HII regions. Indeed, this results in less than 3% difference in the calibration of both channels for the Cygnus region. As we will see, in this work we do not need to go to that precision in the data analysis, since, typical, statistical errors are of order 3-5% also.

We remark that the error associated with the Baars et al. model is dominated by the rather large uncertainty in the spectral indexes  $a$  and  $b$ . However, we have checked that this model predicts flux values for Cygnus A at WMAP frequencies within 10% of the WMAP observed fluxes.

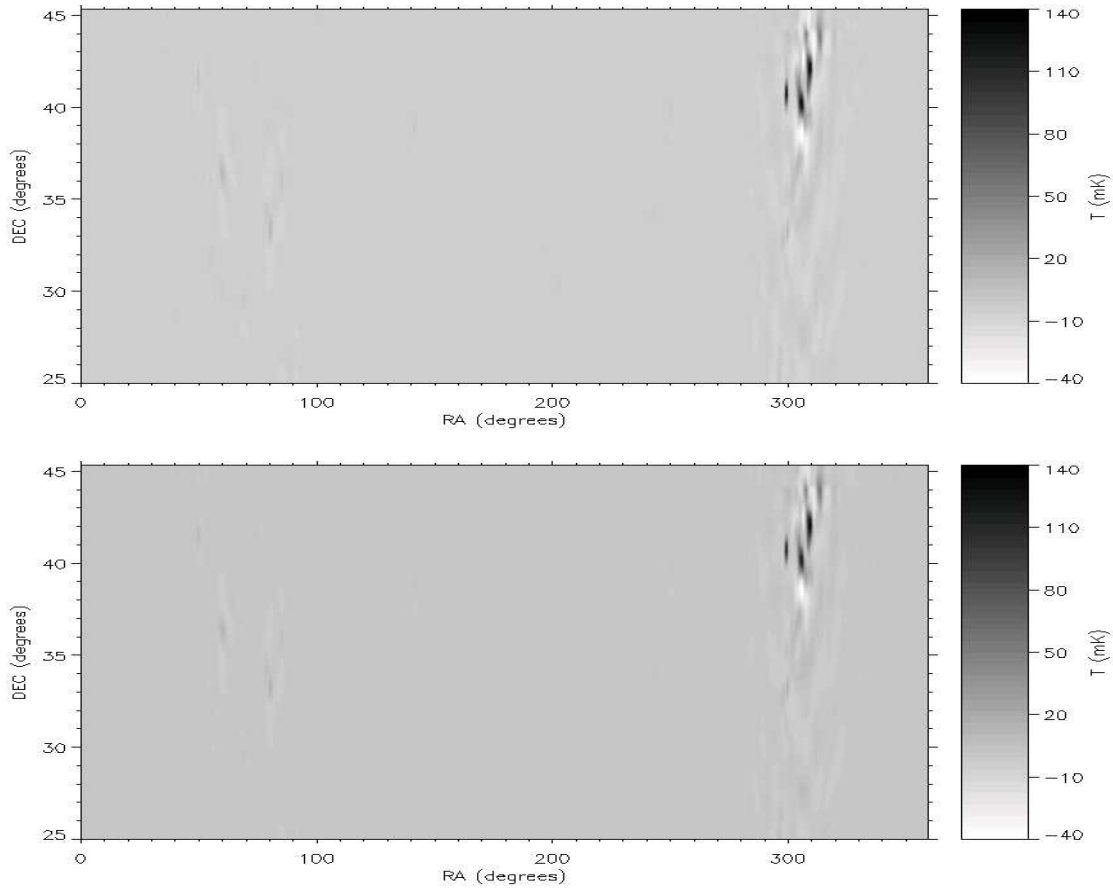
Finally, as an indication, for a good day, the mean RMS of data in regions placed at high Galactic latitude ( $|b| > 50^\circ$ ) is of

order 1.1–1.5 mK, close to the theoretical sensitivity limit of the receivers.

### 3.2 Cumulative maps

In this section, we present the first cumulative maps obtained with the COSMO11 experiment. Maps are pixelized in a rectangular RA and Dec grid. Temperatures for each pixel are computed as the weighted contribution of all the observations relevant to that pixel obtained through the whole observing campaign. The measurements associated to each pixel are weighted each day with the inverse of the variance of the data obtained that day in a  $3^\circ \times 3^\circ$  area centred in the pixel under consideration. This applies to all pixels except those possibly affected by relatively bright radio sources which are treated in a different way. In these cases, the daily weight is taken as the inverse of the variance of the data in high Galactic latitude regions where no strong radio sources are known to contribute. Pixels within the WMAP “Kp0” mask (Bennet et al. 2003) are considered in this category.

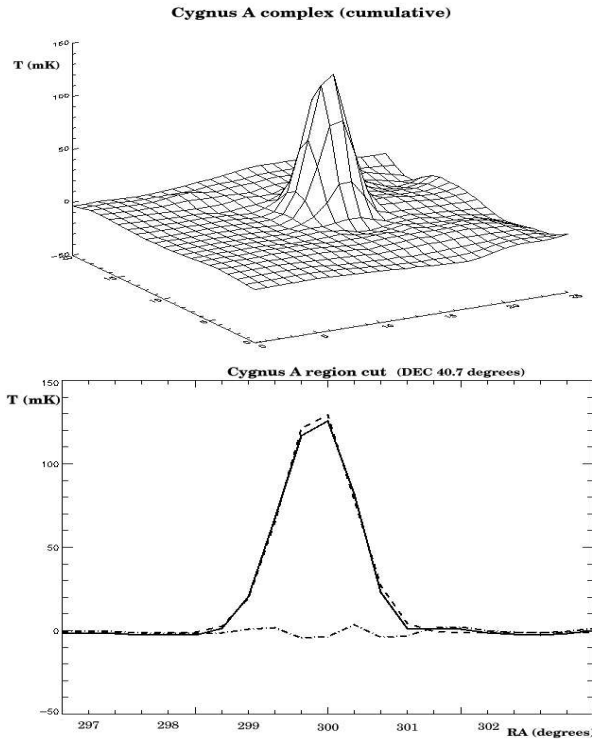
In Fig. 8 we present the final maps of COSMO11 obtained according to the data processing described in Sect. 3.1, i.e., removing a 7<sup>th</sup> order Fourier series along each scan and a 4<sup>th</sup> order one along day-night data to remove atmospheric contamination to the highest possible level. As mentioned in the previous section, the map for channel 1 has the equivalent of 135 days of observations and for channel 2 of 140 days. The angular resolution slightly changes along this map. The values measured for Cygnus A in these two maps, a point source when compared with our beam, are listed in Tab. 3. In the final maps, for the region  $120^\circ \leq \text{RA} \leq 270^\circ$  and  $25^\circ \leq \text{DEC} \leq 45^\circ$ , the RMS per beam (out of the masked regions) is approximately  $52\mu\text{K}$  and  $48\mu\text{K}$  for channel 1 and 2, respectively.



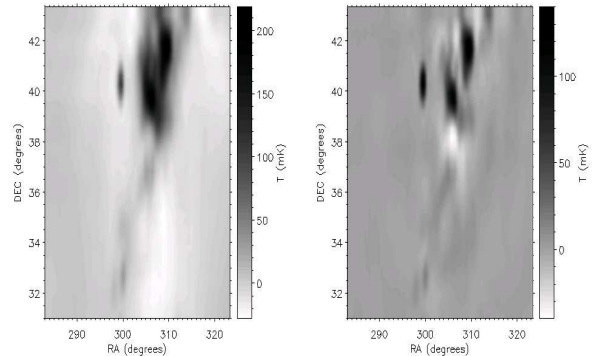
**Figure 8.** Stacked map of COSMO11 channel 1 (top) and channel 2 (bottom) for the period November 2003 to June 2005.

**Table 3.** FWHM in stacked maps for Cygnus A

	FWHM <sub>RA</sub> (°)	FWHM <sub>DEC</sub> (°)
COSMO11 channel 1	$0.80 \pm 0.01$	$1.03 \pm 0.01$
COSMO11 channel 2	$0.80 \pm 0.01$	$1.01 \pm 0.01$

**Figure 9.** Top: Image of the Cygnus A complex for the period November 2003 to June 2005. Bottom: Best 2-dimensional Gaussian fit to Cygnus A (dashed line). Observations (solid line) and difference with the fit (dot-dashed line). Cuts are plotted at the declination of the source.

Finally, as mentioned in Sect. 3.1, the COSMO11 data are not so severely affected by the atmosphere as the COSMO15 data. This may allow a correction of the atmospheric contamination using only low-order harmonics in the Fourier series and thus preserving information on larger angular scales in the final map. In Fig. 10 we show the cumulative map obtained in a region of the Galactic Plane following the same fitting procedure described in Sect. 3.1 but restricted to use only first order harmonics in the Fourier series fit applied to each scan. The resulting maps (similar for both channels) are clearly richer at large scales than the maps constructed with higher order harmonic subtraction. The full exploitation of the information provided by COSMO11 at large scales is left for a future work. Here, we just verified that the values given in Tab. 3 are compatible with those measured in maps generated with atmospheric removal using different number of harmonics in the Fourier series. The result is rather independent on the number of harmonics which is taken as an indication that the implemented source masking procedure works properly for our main calibrator.

**Figure 10.** Left: Galactic plane image in the cumulative map of channel 2 where a 1<sup>st</sup> order Fourier series has been subtracted along each scan. Right: Same, but with the present 7<sup>th</sup> order Fourier series atmospheric subtraction.

### 3.3 Source recognition

A search for radiosources was performed with SExtractor (Bertin & Arnouts 1996) on the map resulting from the combination of the two channels. Some of the brightest point sources are listed in Tab. 3.3 with its most likely identification. The coordinates given in the table are those provided by SExtractor and were used to identify the sources in the Kühr (Kühr et al. 1981), 3C (<http://www.mrao.cam.ac.uk/>) and Green Bank (Gregory et al. 2006) catalogues. We identify each radio source as the brightest source ( $> 1$  Jy) found in these catalogues within 15 arcminutes of the COSMOSOMAS pointing. The 11 GHz fluxes were obtained for these sources as in Fernández-Cerezo et al (2006) by fitting the theoretical point spread function to the COSMO11 data. The errors listed in the table include the calibration uncertainty. The WMAP catalogue was also searched and 22 GHz fluxes are listed whenever available. The sources not found in the WMAP catalogue are either strong steep spectrum sources such as 3C123 or weaker flat spectrum sources such as J2202+4216 which were too faint at the WMAP frequencies to be detected.

Our results are generally consistent with independent observations of these radiosources at similar frequencies (Kühr et al. 1981), except for the source 3C84 for which we give much lower fluxes, but it is well known that the flux of this radiosource has progressively declined in the last few years. The flux measured by COSMO11 is compatible with the tendency delineated by the observations at the UMRAO (Univ. of Michigan Radio Astronomy observatory) in the past decade. Many of the brightest radio sources show large variability and therefore the comparison of fluxes taken in different epochs can only provide a qualitative assessment of our data.

We shall note that our ability to detect point radiosources in the COSMO11 data at high Galactic latitudes is effectively limited to sources with fluxes above  $\sim 1$  Jy due to statistical noise and to the “confusion noise” associated to an unresolved population of extragalactic radio sources. In Fig. 11, a zoom of the final map of COSMO11 shows the detection of several point-like sources near the Galactic plane in the anticenter direction.

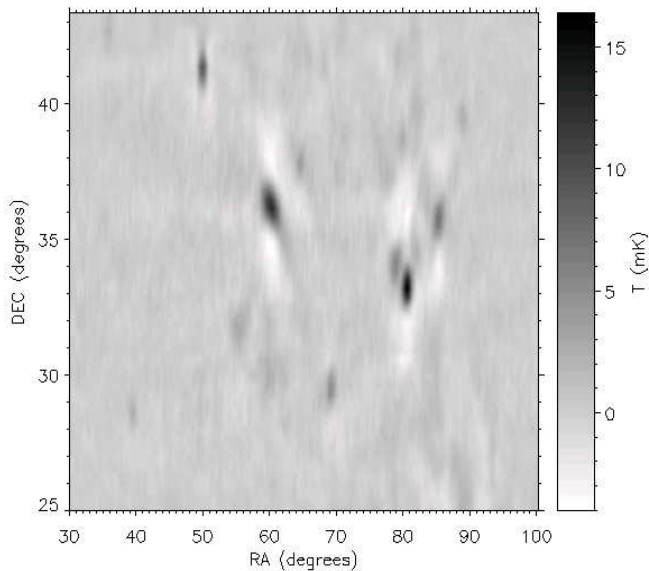
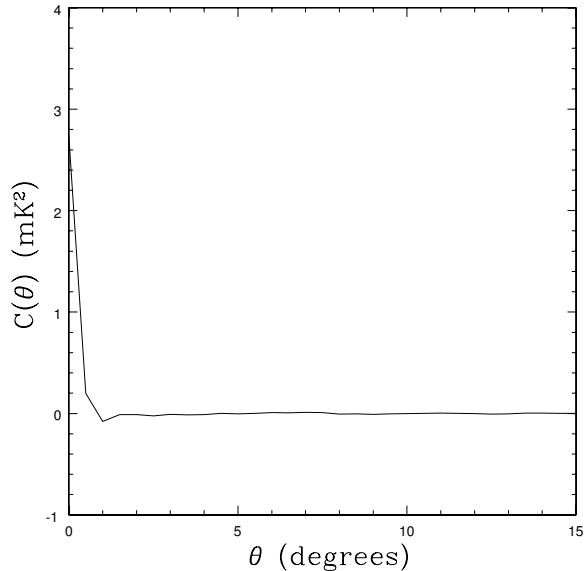
### 3.4 Noise analysis

In this section, we describe the main features of the noise that is still present after subtraction of the first Fourier terms in the daily data. In Fig. 12 we plot the two-point correlation function for a



**Table 4.** A selection of the brightest sources detected in the COSMO11 channels and the corresponding value in the WMAP K channel for comparison.

Source	R.A.	Dec.	Channel 1 flux (Jy)	Channel 2 flux(Jy)	WMAP K
3C84	50.16	41.54	$16.6 \pm 1.7$	$17.8 \pm 1.8$	11.1
3C123	69.18	29.33	$14.0 \pm 1.4$	$13.7 \pm 1.4$	—
0923+39	141.91	38.89	$10.2 \pm 1.0$	$10.8 \pm 1.1$	6.8
J0418+3801	64.64	38.08	$9.5 \pm 1.0$	$9.0 \pm 0.9$	—
3C345	250.74	39.86	$8.6 \pm 0.9$	$9.2 \pm 1.0$	8.0
J0555+3948	89.17	39.79	$3.9 \pm 0.4$	$4.7 \pm 0.5$	1.2
3C465	354.73	26.65	$3.2 \pm 0.4$	$3.5 \pm 0.4$	—


**Figure 11.** A section of the final map of COSMO11 (channel 1) showing the detection of point-like sources towards the Galactic anticenter.

**Figure 12.** Two-point correlation function for a single day in COSMO11.

representative day. This is performed in a region  $RA=(115^\circ, 267^\circ)$ ,  $DEC=(25^\circ, 45^\circ)$  that corresponds to high Galactic latitude and using the source mask described in Sect. 4.

Some degree of correlation is expected between channels observing simultaneously the same sky region. As mean covariance of the data of the two channels, we have obtained the average of the two-point correlation functions computed for each day whenever simultaneous observations in both channels were available (98 % of the days). The result is 0.40 mK, whereas the typical daily RMS of the data is 2.25 mK and 1.96 mK for channel 1 and 2, respectively. For comparison, the correlation between different days was found to be less than 1 % in good agreement with expectations for the amplitude of the astronomical signals.

### 3.4.1 Stacked maps

Finally, we have also considered the evolution of the noise per pixel when stacking daily maps. We verified that the RMS of the data contributing to each pixel decreased roughly as  $1/\sqrt{N}$ , where  $N$  is the number of stacked daily maps. In the final maps of channel 1 and 2, the typical errors in temperature (per pixel) are of order 130–140  $\mu$ K.

## 4 DATA ANALYSIS

In this section, we study the degree of correlation of the previous two COSMO11 stacked maps with multifrequency datasets available in the literature for the same sky region. The goal is to establish the contribution of CMB, synchrotron, brehmstrahlung, extragalactic radiosources and anomalous microwave emission at the frequency and angular scales of our experiment. The set of maps to be correlated with COSMO11 are: (i) the 3rd year maps for each of the five channels of the WMAP mission (Hinshaw et al. 2007)<sup>3</sup>; (ii) the extragalactic radiosource emission maps constructed from the NVSS catalogue; (iii) the 408 MHz map provided by (Haslam et al. 1982); (iv) the  $H_\alpha$  map provided by (Finkbeiner 2003); and (v) the DIRBE maps at 100  $\mu$ m (DIRBE08) and 240  $\mu$ m (DIRBE10), and a HEALPix version of the dust map provided by (Schlegel et al. 1998) from LAMBDA<sup>4</sup> at 100  $\mu$ m, ( $\Lambda_{100}$  in the sequel).

The method used for the computation of the correlation between maps is described in detail in de Oliveira-Costa et al. (2004) and Fernández-Cerezo et al. (2006). Correlation coefficients can be computed by comparison with just one template map or simultaneously with several maps. The multi-correlation option is preferred

<sup>3</sup> These maps are given in the HEALPix pixelisation scheme (Górski et al. 2005).

<sup>4</sup> <http://lambda.gsfc.nasa.gov/>.

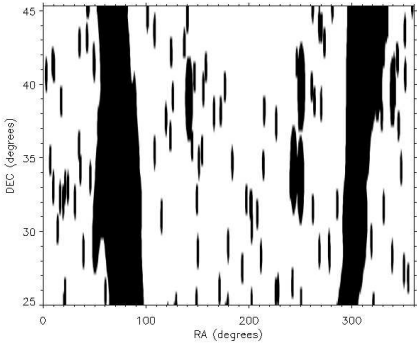


**Figure 13.** Mask used for the cross-correlation studies, see text for details.

when the templates present some degree of correlation themselves, as it is the case of those describing Galactic emission processes. In this work, all the correlation results except those corresponding to CMB come from a multi correlation analysis (unless otherwise stated) where the templates considered are: i) the V channel of the WMAP mission for CMB, ii) the NVSS map, iii) the 408 MHz map, iv) the  $H_\alpha$  map and v) any of the three dust maps mentioned before.

The correlation study considers data between  $25.0^\circ \leq \text{DEC} \leq 44.7^\circ$  as allowed by the mask plotted in Fig. 13. This is an extended version of the “Kp0” mask used by WMAP where any adjacent pixel was also discarded for the correlation. Additionally, we masked some regions at high galactic latitude with strong radiosources to minimize any possible residual effects of these sources after the adopted atmospheric filtering. The regions masked are (RA;DEC):  $(141.7^\circ \pm 3.7^\circ, 38.7^\circ \pm 2.7^\circ)$ ,  $(243.0^\circ \pm 3.7^\circ, 34.3^\circ \pm 3.3^\circ)$ ,  $(250.7^\circ \pm 3.7^\circ, 33.5^\circ \pm 3.3^\circ)$ ,  $(250.7^\circ \pm 3.7^\circ, 39.7^\circ \pm 2.7^\circ)$ .

Several other masking criteria were also considered in the correlation analysis: excluding all additional sources for which a direct extrapolation of the fluxes in the NVSS and GB6 catalogues yielded values higher than 1 Jy at 11 GHz; extending the Kp0 by two or three pixels around each masked source; and finally, excluding any pixels with temperatures deviating several times the typical error per pixel of the map. The correlation results obtained with the various masks agreed within the statistical error bars of the method.

In the following sections we deal with  $1\sigma$  statistical errors estimated directly from the correlation method, but other sources of error should also be considered. Absolute calibration errors amount up to 10 % and chance alignment of regions with emission caused by physically unrelated processes also contribute to the final uncertainties. To determine the role of chance alignment, we have computed the correlation values and their dispersion for arbitrary rotations of the templates around an axis perpendicular to the Galactic plane. The dispersions of the correlation values were found usually 1–2 times higher than the statistical error given by the correlation method. Only those correlation values larger than 2 times the statistical error will be considered a reliable result.

The COSMO11 maps are convolved to a final angular resolution of  $1.12^\circ \times 1.12^\circ$  to set on equal foot the COSMO11 and COSMO15 data, so both experiments can be compared directly. We have not considered the different polarization of the two COSMO11 channels in producing the set of templates. This may lead to systematic differences in the correlation results obtained for each channel with the same templates. In general, these differences

will not be larger than a few percent of the amplitude of the correlated signals, i.e. smaller than the statistical error of the correlation method.

With the adopted atmospheric filtering, the window function describing the data of the COSMO11 radiometer is analogous to that published by Fernández-Cerezo et al. (2006) for COSMO15. We remark that the filtering applied to the COSMOSOMAS data during the reduction process is also applied to any other map used in the correlation analysis. This erases information on the largest scales, so the results need to be understood as the correlation level at the remaining scales, which essentially range from  $\sim 1^\circ$  to  $5^\circ$ . Finally, here we have reprocessed the COSMO15 data obtained by Fernández-Cerezo et al. (2006), according to the procedures explained in Sect. 2.4 which are slightly different to those used in the former work. The cross-correlation results obtained for the COSMO15 data are also slightly different.

#### 4.1 Correlations with WMAP data

In Tab. 5 we list the correlation values obtained for the COSMOSOMAS (labelled as C11<sub>1</sub> and C11<sub>2</sub> for the two COSMO11 channels, and C13, C15 and C16 for the three COSMO15 channels) and the WMAP channels for three different galactic latitude cuts. First, we note that the correlations among the highest frequency channels of WMAP indicate the level of the CMB signal left by the window function associated to the adopted COSMOSOMAS data processing scheme. The correlations between the Q, V and W channels show a detection of CMB with amplitude 26–26.5  $\mu\text{K}$  at the various Galactic latitude cuts. This is in agreement with the expected CMB fluctuation after removal of the Fourier terms described in Sect. 3.1. The autocorrelation values for these channels are  $\sim 0.5 \mu\text{K}$  higher as expected for the noise contribution.

Approximately the same level of correlation (26–29  $\mu\text{K}$ ) is found between the five COSMOSOMAS channels, and the high frequency WMAP channels (see Fig. 14). The CMB signal is detected in both COSMO11 channels with a high significance ( $> 25\sigma$ ). CMB polarization is expected to cause differences between the correlation values obtained for each of the two COSMO11 channels smaller than the statistical uncertainties. Therefore no attempt was made to measure this polarization effect in our data. When we consider regions at low Galactic latitude, as e.g.  $|b| > 30^\circ$ , the amplitude of the CMB correlated signal slightly decreases, this is an artifact due to the strong influence of the Galactic plane signal which affects the processing of COSMOSOMAS data.

The amplitude of the correlated signal between COSMO11 and the low-frequency WMAP channels increases to  $\sim 43$  and 35  $\mu\text{K}$ , for the K and K<sub>a</sub> channels ( $|b| > 40^\circ$ ), respectively. This is attributed to signals in common other than CMB. At high galactic latitude and considering the angular scales relevant to the present analysis, the expected major foreground contamination in common with these WMAP channels are unresolved extragalactic radiosources as we will see in the next sections.

#### 4.2 Correlations with unresolved radio sources

In order to determine the level of the contribution of unresolved radio sources in the COSMOSOMAS data we proceed as in Fernández-Cerezo et al. (2006). Essentially, for each galactic latitude and at each frequency the correlation values of COSMOSOMAS with the WMAP K map (values of Tab. 5) are corrected from the CMB contribution (obtained as mentioned above), as well as

**Table 5.** Values of the temperature correlation in  $\mu\text{K}$  for the COSMO11 cumulative map with respect to the maps of the five WMAP channels for different cuts in Galactic latitude,  $b$ . Errors are  $1\sigma$ .

Template	C11 <sub>1</sub>	C11 <sub>2</sub>	C13	C15	C16	WMAP-K	WMAP-Ka	WMAP-Q	WMAP-V	WMAP-W
$ b  > 30^\circ$										
WMAP-K	$42.5 \pm 0.9$	$43.8 \pm 0.8$	$32.1 \pm 1.0$	$30.9 \pm 1.2$	$31.9 \pm 3.0$	$29.3 \pm 0.1$	$26.0 \pm 0.1$	$25.3 \pm 0.1$	$24.7 \pm 0.1$	$24.4 \pm 0.1$
WMAP-Ka	$33.0 \pm 0.9$	$34.0 \pm 0.8$	$27.3 \pm 1.0$	$26.3 \pm 1.2$	$28.4 \pm 3.0$	$28.0 \pm 0.1$	$27.4 \pm 0.1$	$26.5 \pm 0.1$	$26.2 \pm 0.1$	$26.0 \pm 0.1$
WMAP-Q	$29.9 \pm 0.9$	$31.1 \pm 0.8$	$26.1 \pm 1.0$	$25.5 \pm 1.2$	$27.7 \pm 3.0$	$27.5 \pm 0.1$	$26.8 \pm 0.1$	$27.0 \pm 0.1$	$26.4 \pm 0.1$	$26.2 \pm 0.1$
WMAP-V	$27.0 \pm 0.9$	$27.7 \pm 0.8$	$23.9 \pm 1.0$	$23.9 \pm 1.2$	$25.0 \pm 3.0$	$26.9 \pm 0.1$	$26.5 \pm 0.1$	$26.4 \pm 0.1$	$26.9 \pm 0.1$	$26.2 \pm 0.1$
WMAP-W	$25.1 \pm 0.9$	$25.7 \pm 0.8$	$23.0 \pm 1.0$	$23.5 \pm 1.2$	$24.9 \pm 3.0$	$26.5 \pm 0.1$	$26.3 \pm 0.1$	$26.2 \pm 0.1$	$26.2 \pm 0.1$	$27.0 \pm 0.1$
$ b  > 40^\circ$										
WMAP-K	$42.7 \pm 1.0$	$44.1 \pm 0.9$	$34.2 \pm 1.1$	$32.8 \pm 1.4$	$33.3 \pm 3.5$	$29.1 \pm 0.2$	$25.8 \pm 0.2$	$25.2 \pm 0.1$	$24.7 \pm 0.1$	$24.4 \pm 0.1$
WMAP-Ka	$34.4 \pm 1.0$	$35.6 \pm 0.9$	$29.9 \pm 1.1$	$28.3 \pm 1.4$	$29.9 \pm 3.5$	$27.7 \pm 0.2$	$27.1 \pm 0.2$	$26.2 \pm 0.1$	$26.0 \pm 0.1$	$25.8 \pm 0.1$
WMAP-Q	$31.7 \pm 1.0$	$33.1 \pm 0.9$	$28.8 \pm 1.1$	$28.0 \pm 1.4$	$29.6 \pm 3.5$	$27.4 \pm 0.2$	$26.5 \pm 0.2$	$26.7 \pm 0.1$	$26.3 \pm 0.1$	$26.1 \pm 0.1$
WMAP-V	$29.0 \pm 1.0$	$29.7 \pm 0.9$	$26.9 \pm 1.1$	$26.5 \pm 1.4$	$27.2 \pm 3.5$	$26.8 \pm 0.2$	$26.3 \pm 0.2$	$26.2 \pm 0.1$	$26.8 \pm 0.1$	$26.1 \pm 0.1$
WMAP-W	$27.3 \pm 1.0$	$28.1 \pm 0.9$	$26.1 \pm 1.1$	$26.0 \pm 1.4$	$27.3 \pm 3.5$	$26.4 \pm 0.2$	$26.1 \pm 0.2$	$26.0 \pm 0.1$	$26.1 \pm 0.1$	$26.8 \pm 0.1$
$ b  > 50^\circ$										
WMAP-K	$41.1 \pm 1.1$	$41.3 \pm 1.0$	$33.6 \pm 1.3$	$31.0 \pm 1.6$	$33.5 \pm 3.9$	$29.3 \pm 0.2$	$26.3 \pm 0.2$	$25.8 \pm 0.1$	$25.3 \pm 0.1$	$25.0 \pm 0.1$
WMAP-Ka	$34.2 \pm 1.1$	$34.3 \pm 1.0$	$29.9 \pm 1.3$	$26.9 \pm 1.6$	$30.6 \pm 3.9$	$28.1 \pm 0.2$	$27.4 \pm 0.2$	$26.7 \pm 0.1$	$26.5 \pm 0.1$	$26.2 \pm 0.1$
WMAP-Q	$31.6 \pm 1.1$	$32.1 \pm 1.0$	$28.9 \pm 1.3$	$26.7 \pm 1.6$	$30.7 \pm 3.9$	$27.8 \pm 0.2$	$26.9 \pm 0.2$	$27.1 \pm 0.1$	$26.6 \pm 0.1$	$26.4 \pm 0.1$
WMAP-V	$29.1 \pm 1.1$	$29.0 \pm 1.0$	$27.2 \pm 1.3$	$25.3 \pm 1.6$	$28.4 \pm 3.9$	$27.3 \pm 0.2$	$26.7 \pm 0.2$	$26.7 \pm 0.1$	$27.1 \pm 0.1$	$26.4 \pm 0.1$
WMAP-W	$28.0 \pm 1.1$	$27.9 \pm 1.0$	$26.9 \pm 1.3$	$25.7 \pm 1.6$	$29.0 \pm 3.9$	$26.9 \pm 0.2$	$26.5 \pm 0.2$	$26.5 \pm 0.1$	$26.5 \pm 0.1$	$27.1 \pm 0.1$

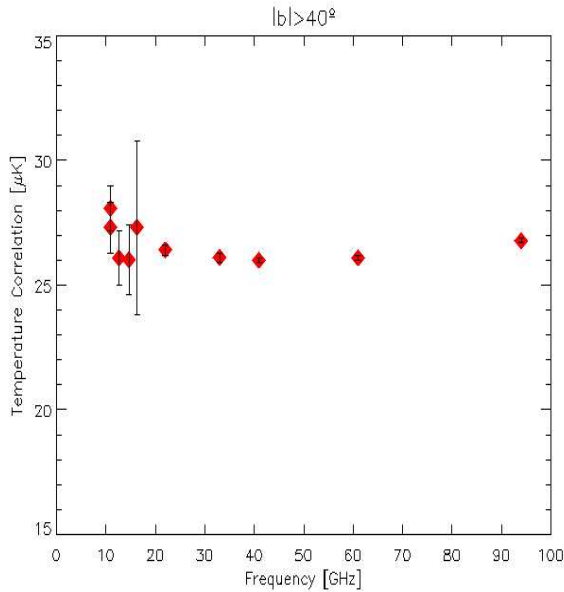


**Figure 14.** Correlation of COSMOSOMAS and WMAP channels with the V channel of WMAP. Error bars are  $1\sigma$  statistical errors.

from the corresponding correlation with the Galactic synchrotron (408 MHz map), free-free ( $H\alpha$  template) and dust (DIRBE08) (see next sections for details on these correlations and their statistical errors). The correction consists in a subtraction of each of the previous temperature correlation values in quadrature. We obtain the results listed in Tab. 6 and plotted in Fig. 15. The data point at 23 GHz in Fig. 15 is obtained correcting the autocorrelation value of the WMAP K for the contribution of the CMB and the other foregrounds. It is clear the existence of an additional signal in common between the COSMOSOMAS data and WMAP K band whose amplitude is independent of galactic latitude and decreases with increasing frequency. At the frequencies of COSMOSOMAS and at the angular scales under consideration, this additional signal turns out to be the second most relevant contribution (after CMB) to the temperature fluctuations at high Galactic latitudes.

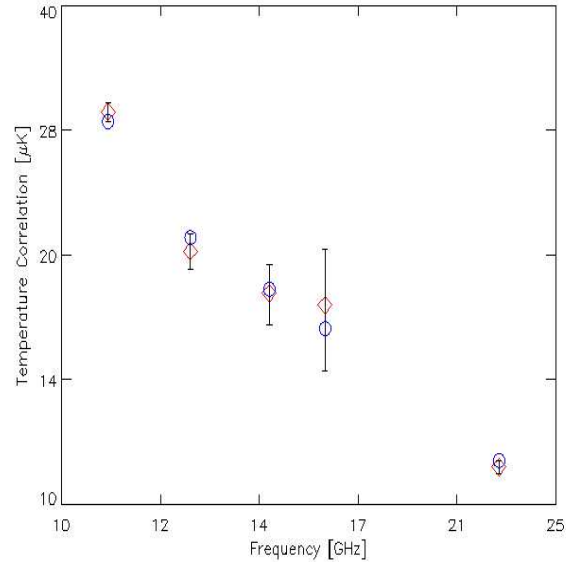


**Figure 15.** Predicted (circles) and observed (diamonds) contribution from unresolved radio sources, after taking into account COSMOSOMAS observing strategy and data processing. See text, and Tab. 6 for details.

In order to interpret these results we use the models by de Zotti et al. (2005) and estimate the expected contribution of unresolved radio sources. Assuming a detection limit of 1 Jy for resolved radio sources (masked in our correlation analysis) and considering our window function these models predict at 11 GHz a total contribution of unresolved radio sources of order  $29.0\ \mu\text{K}$  (González-Nuevo private communication). For the COSMO15 frequencies the models predict contributions of order  $21.0\ \mu\text{K}$ ,  $18.2\ \mu\text{K}$ ,  $16.3\ \mu\text{K}$  for C13, C15, and C17 channels, respectively. Finally, for the WMAP K channel, the predicted contribution is of order  $11.3\ \mu\text{K}$ . The excess temperature correlation values in Tab. 6 agree remarkably well with these model predictions. Both are compared in Fig. 15.

**Table 6.** Temperature cross correlation excess between the COSMOSOMAS and WMAP K map after contributions from CMB and Galactic emission are accounted, see text for details. All the maps are processed according to COSMOSOMAS strategy. Errors are  $1 \sigma$ . The error bars are computed taking into account the error bars of each correlation and the cross correlation between templates.

Template	C11 <sub>1</sub>	C11 <sub>2</sub>	C13	C15	C16	WMAP_K
$ b  > 30^\circ$						
Excess of signal	$30.0 \pm 1.9$	$30.6 \pm 1.7$	$20.1 \pm 2.0$	$18.4 \pm 2.5$	$18.1 \pm 4.9$	$11.3 \pm 0.4$
$ b  > 40^\circ$						
Excess of signal	$30.2 \pm 1.9$	$31.0 \pm 1.8$	$21.0 \pm 2.0$	$18.7 \pm 2.8$	$18.2 \pm 5.1$	$11.1 \pm 0.4$
$ b  > 50^\circ$						
Excess of signal	$28.4 \pm 2.0$	$28.8 \pm 1.8$	$19.5 \pm 2.2$	$16.9 \pm 2.9$	$16.0 \pm 4.9$	$10.7 \pm 0.5$

### 4.3 Correlations with 408 MHz and 1420 MHz data

In the upper section of Tab. 7 we list the correlation values between COSMOSOMAS, WMAP and the 408 MHz template. Significant correlations are found at the three Galactic latitude cuts at all frequencies. The map at 408 MHz is regarded as a good tracer of synchrotron at large scales. However, at the angular scales left by the atmospheric filtering in the COSMOSOMAS data processing, the 408 MHz template includes a significant contribution from extragalactic radiosources as can be seen from direct comparison with the NVSS template plotted in Fig. 16, see also (Burigana et al. 2006). In order to disentangle the contribution of extragalactic radiosources and Galactic synchrotron at high Galactic latitude, we performed a simultaneous multi-correlation analysis including the NVSS template. The results are given in the lower section of Tab. 7 and are interpreted as evidence for a rather weak Galactic synchrotron signal left at our angular scales. Although, the dispersion of the values is high for a precise determination of the synchrotron spectral index, the results between 11 GHz and 22.5 GHz are compatible with a temperature spectral index of -3, characteristic of synchrotron emission.

We have also studied the correlation of our maps with a desourced (Ds) Haslam et al. map given by the LAMBDA archive<sup>5</sup>. The results improve in the sense that a lower correlation with NVSS is found, but synchrotron is still dominated by extragalactic radio sources at our angular scales. A very similar conclusion follows when using 1420 MHz data (Reich & Reich 1982). Finally, we have built a COSMO11 Q map, combining the data from the two channels, and performed a cross-correlation with the Wollaben et al. (2006) Q map at 1420 MHz. The potential signals are at the level of the statistical errors in the cross-correlation and therefore no conclusion could be drawn for a polarized Galactic synchrotron signal at 11 GHz. An upper limit on the polarization level is set at  $2 \mu\text{K}$  (68 % C.L.).

### 4.4 Correlations with $H\alpha$ data

Free-free emission is a likely contributor at our observing frequencies, especially relevant when discussing any possible dust correlated emission. At high Galactic latitudes, absorption corrections can be ignored at first order and we adopt the combined map of  $H\alpha$  emission provided by (Finkbeiner 2003) as an accurate enough tracer of free-free emission. Tab. 8 gives the temperature correlation coefficient between COSMOSOMAS and WMAP data and

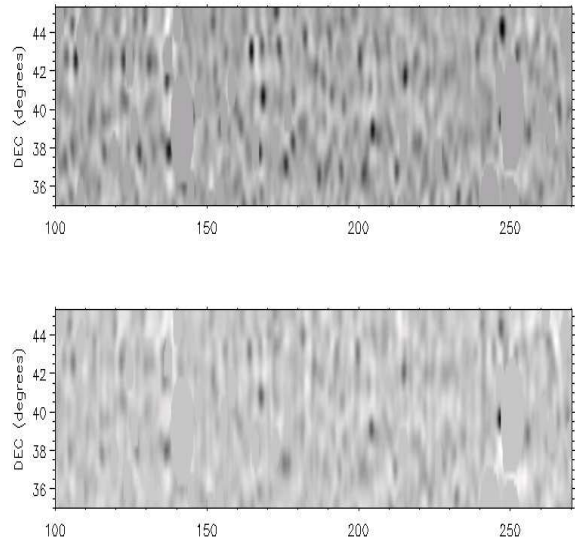


**Figure 16.** A visual comparison between the NVSS map (top) and the 408 MHz map (bottom) when processed according to COSMOSOMAS strategy and degraded to a common 1 degree angular resolution.

this  $H\alpha$  map filtered according to the COSMOSOMAS data processing. From the table, we obtain a conversion from Rayleighs to K of order  $40\text{--}60 \mu\text{K/R}$  for both channels of COSMO11. Theoretical predictions (Dickinson et al. 2003, Bennet et al. 2003) for high Galactic latitude yield, assuming a mean electron temperature of  $7000\text{--}8000 \text{ K}$ ,  $51\text{--}55 \mu\text{K/R}$  at  $10.9 \text{ GHz}$ . This is compatible with our results.

### 4.5 Correlations with dust data

The temperature correlations between COSMOSOMAS/WMAP and several dust templates are shown in Tab. 9 for various Galactic latitude cuts. These results are obtained with the multifit scheme described above. We have verified that they change by less than  $\sim 1 \mu\text{K}$  with respect performing a simple one to one correlation between the COSMOSOMAS and WMAP data and the dust templates. Within statistical errors the results are also independent on the templates used in the multifit.

For  $|b| > 30^\circ$ , the most significant correlations are obtained

<sup>5</sup> [http://lambda.gsfc.nasa.gov/product/foreground/haslam\\_408.cfm](http://lambda.gsfc.nasa.gov/product/foreground/haslam_408.cfm)

**Table 7.** Temperature cross correlation between the COSMOSOMAS and WMAP maps and the 408 MHz map. The first table is for a single correlation analysis. The second one for the multifit case where NVSS is included in the list of templates. The reduction in the amplitude of the correlation values is due exclusively to the inclusion of the NVSS template in the fit. Errors are  $1 \sigma$ .

Template	C11 <sub>1</sub>	C11 <sub>2</sub>	C13	C15	C16	WMAP_K	WMAP_Ka	WMAP_Q	WMAP_V	WMAP_W
$ b  > 30^\circ$										
408 MHz	<b>23.6 ± 0.9</b>	<b>24.0 ± 0.8</b>	<b>11.9 ± 0.9</b>	<b>8.1 ± 1.2</b>	4.6 ± 2.8	<b>3.5 ± 0.2</b>	<b>1.5 ± 0.2</b>	<b>0.9 ± 0.2</b>	<b>0.7 ± 0.2</b>	0.1 ± 0.2
$ b  > 40^\circ$										
408 MHz	<b>25.1 ± 1.0</b>	<b>26.3 ± 0.9</b>	<b>11.5 ± 1.1</b>	<b>7.6 ± 1.4</b>	3.5 ± 3.4	<b>3.9 ± 0.2</b>	<b>1.7 ± 0.2</b>	<b>1.1 ± 0.2</b>	<b>0.9 ± 0.2</b>	0.3 ± 0.2
$ b  > 50^\circ$										
408 MHz	<b>23.1 ± 1.1</b>	<b>24.0 ± 1.0</b>	<b>9.5 ± 1.2</b>	<b>4.3 ± 1.5</b>	1.9 ± 3.7	<b>4.4 ± 0.3</b>	<b>2.4 ± 0.3</b>	<b>1.6 ± 0.2</b>	<b>1.3 ± 0.2</b>	<b>1.0 ± 0.2</b>

Template	C11 <sub>1</sub>	C11 <sub>2</sub>	C13	C15	C16	WMAP_K	WMAP_Ka	WMAP_Q	WMAP_W
$ b  > 30^\circ$									
408 MHz	<b>2.8 ± 1.0</b>	<b>2.8 ± 0.9</b>	1.1 ± 1.1	-1.3 ± 1.4	-5.4 ± 3.3	0.0 ± 0.3	-0.1 ± 0.3	-0.1 ± 0.3	-0.4 ± 0.3
$ b  > 40^\circ$									
408 MHz	<b>5.6 ± 1.2</b>	<b>6.0 ± 1.1</b>	1.0 ± 1.3	-2.2 ± 1.7	-6.2 ± 4.0	0.1 ± 0.3	-0.2 ± 0.3	-0.2 ± 0.3	-0.5 ± 0.3
$ b  > 50^\circ$									
408 MHz	<b>4.2 ± 1.3</b>	<b>4.7 ± 1.2</b>	-0.6 ± 1.5	<b>-5.0 ± 1.8</b>	-5.4 ± 4.3	0.3 ± 0.4	0.2 ± 0.4	-0.1 ± 0.3	-0.3 ± 0.4

**Table 8.** Values of the temperature correlation in  $\mu\text{K}$  between COSMOSOMAS/WMAP and the  $\text{H}\alpha$  map for different cuts in Galactic latitude,  $b$ . Errors are  $1 \sigma$ .

Template	C11 <sub>1</sub>	C11 <sub>2</sub>	C13	C15	C16	WMAP_K	WMAP_Ka	WMAP_Q	WMAP_W
$ b  > 30^\circ$									
$\text{H}\alpha$	<b>6.4 ± 0.9</b>	<b>6.8 ± 0.8</b>	<b>4.1 ± 0.9</b>	<b>2.5 ± 1.2</b>	-1.7 ± 2.9	<b>0.9 ± 0.3</b>	0.3 ± 0.3	0.0 ± 0.2	0.0 ± 0.2
$ b  > 40^\circ$									
$\text{H}\alpha$	<b>2.7 ± 1.0</b>	<b>2.1 ± 0.9</b>	1.0 ± 1.2	<b>4.0 ± 1.5</b>	0.2 ± 3.5	0.4 ± 0.3	0.3 ± 0.3	0.1 ± 0.3	0.0 ± 0.3
$ b  > 50^\circ$									
$\text{H}\alpha$	<b>4.0 ± 1.2</b>	<b>3.2 ± 1.1</b>	-1.6 ± 1.3	2.7 ± 1.7	-1.8 ± 3.9	0.2 ± 0.3	0.1 ± 0.3	-0.1 ± 0.3	-0.1 ± 0.3

**Table 9.** Values of the temperature correlation between the COSMOSOMAS/WMAP maps and dust maps for different Galactic latitudes. The values are obtained from a multifit, see text. Errors are  $1 \sigma$ .

Template	1420 MHz	C11 <sub>1</sub>	C11 <sub>2</sub>	C13	C15	C16	WMAP_K	WMAP_Ka	WMAP_Q	WMAP_W
$ b  > 30^\circ$										
$\Lambda 100$	525.1 ± 569.1	<b>9.1 ± 0.9</b>	<b>10.1 ± 0.8</b>	<b>4.4 ± 0.9</b>	<b>4.9 ± 1.1</b>	<b>7.0 ± 2.7</b>	<b>2.7 ± 0.3</b>	<b>0.7 ± 0.3</b>	0.3 ± 0.2	-0.1 ± 0.2
DIRBE08	518.0 ± 578.1	<b>11.4 ± 0.9</b>	<b>12.5 ± 0.8</b>	<b>5.8 ± 0.9</b>	<b>6.3 ± 1.2</b>	<b>5.9 ± 2.9</b>	<b>2.8 ± 0.3</b>	<b>0.7 ± 0.3</b>	0.3 ± 0.2	-0.2 ± 0.2
DIRBE10	616.0 ± 566.1	<b>9.7 ± 0.9</b>	<b>11.3 ± 0.8</b>	<b>3.7 ± 0.9</b>	1.9 ± 1.2	5.2 ± 2.9	<b>2.1 ± 0.3</b>	0.5 ± 0.3	0.2 ± 0.2	-0.3 ± 0.2
$ b  > 40^\circ$										
$\Lambda 100$	-617.0 ± 663.0	<b>6.2 ± 1.0</b>	<b>7.2 ± 1.0</b>	0.4 ± 1.2	<b>3.4 ± 1.4</b>	1.5 ± 3.5	<b>1.5 ± 0.3</b>	<b>0.6 ± 0.3</b>	0.3 ± 0.3	0.1 ± 0.3
DIRBE08	-955.0 ± 663.0	<b>6.1 ± 1.1</b>	<b>7.4 ± 1.0</b>	1.0 ± 1.2	2.3 ± 1.4	0.0 ± 3.5	<b>1.2 ± 0.3</b>	0.5 ± 0.3	0.2 ± 0.3	0.0 ± 0.3
DIRBE10	-314.0 ± 657.1	<b>4.7 ± 1.0</b>	<b>6.2 ± 0.9</b>	1.4 ± 1.2	-0.7 ± 1.5	-0.6 ± 3.5	<b>0.8 ± 0.3</b>	0.3 ± 0.3	0.2 ± 0.3	-0.1 ± 0.3
$ b  > 50^\circ$										
$\Lambda 100$	<b>-1487.0 ± 732.1</b>	<b>2.6 ± 1.2</b>	1.8 ± 1.1	<b>2.6 ± 1.3</b>	<b>3.6 ± 1.6</b>	-2.8 ± 4.0	<b>1.4 ± 0.3</b>	0.5 ± 0.3	0.3 ± 0.3	0.2 ± 0.3
DIRBE08	<b>-1660.0 ± 731.1</b>	1.6 ± 1.2	1.6 ± 1.1	<b>2.6 ± 1.3</b>	2.0 ± 1.6	-5.0 ± 4.0	<b>0.9 ± 0.3</b>	0.4 ± 0.3	0.2 ± 0.3	0.0 ± 0.3
DIRBE10	-651.1 ± 723.0	<b>2.8 ± 1.1</b>	<b>4.4 ± 1.0</b>	<b>3.6 ± 1.3</b>	0.2 ± 1.6	-5.0 ± 3.9	<b>0.8 ± 0.3</b>	0.2 ± 0.3	0.2 ± 0.3	-0.1 ± 0.3

for both COSMO11 channels, with a signal to noise ratio greater than 10, and for the WMAP K channel, with a signal to noise around 7–9. Marginal detections are also found with the Ka channel. No significant detection is found at the higher frequency channels of WMAP. The channels of COSMO15 also exhibit some clear detections, although for some templates these are less significant. At higher Galactic latitudes the amplitude of the correlated signal decreases and for  $|b| > 50^\circ$  the detections are below the  $3\sigma$  level. Overall, we find clear evidence for a dust correlated high Galactic latitude microwave emission in the frequency range 11–33 GHz.

We note that the two COSMO11 channels present a small systematic difference in the values of the correlations at  $|b| > 30^\circ$  and  $|b| > 40^\circ$ , of order  $1\text{--}1.5 \mu\text{K}$ , similar to the statistical error. In principle, this could be due to a significant level of polarization in the dust-correlated signal but more sensitive maps are required in order to establish whether this is a reliable difference.

The dust-correlated signal detected in Tab. 9 presents a spectral index between 11 and 33 GHz of  $-2.1 \pm 0.2$ , incompatible with synchrotron emission ( $\sim -3$ ) but consistent with free-free emission. However, the remarkable flattening found in the frequency range of the COSMOSOMAS experiment cannot be understood in terms of free-free emission properly, suggesting an improper tracing of the free-free emission at high Galactic latitude by the  $\text{H}\alpha$  template used in the multifit analysis. This would be the case in regions of high dust emission where dust also causes high extinction in the visual. A careful study of the regions that mostly contribute to the dust-correlated signal in the COSMO11 data at  $|b| > 30^\circ$  reveals areas with a very strong emission in the DIRBE maps which indeed are not  $\text{H}\alpha$  emitters. Dust extinction in these regions would cause that free-free emission would not be traced by the  $\text{H}\alpha$  template affecting to the correlation values listed in Tab. 9. In order to explore if this is the case, we identified regions with very strong dust emission at high Galactic latitudes and performed a new correlation study by extending the mask to include those pixels with a significant correlated emission with the COSMOSOMAS maps. For definiteness, we extended the mask to those pixels where the amplitude of the normalised covariance between the channel 2 of COSMOSOMAS (the one with the best sensitivity) and DIRBE08 (i.e.  $\langle t_{C2} t_{D08} \rangle / (\sigma(t_{C2}) \sigma(t_{D08}))$ ) was greater than 5. Adjacent pixels were also masked. In total, only a few regions of size 1 – 5 square degrees were removed from the analysis and a new multifit correlation analysis was performed. The results are listed in Tab. 10. We find a decrease in the amplitude of the dust-correlated signal at any frequency with respect to the case in Tab. 9 but the correlations at  $|b| > 30^\circ$  are very significant for COSMO11 and WMAP\_K and significant for the other COSMOSOMAS channels. There is also a trend to lower amplitudes as we move to high Galactic latitude. In order to see if this dust-correlated microwave emission could be associated with synchrotron, free-free or a different emission process we conducted a detailed analysis of the DIRBE08 correlation values listed in Tab. 10 for  $|b| > 30^\circ$ .

A maximum likelihood approach has been used to find the best-fit parameters within three different models. First, we considered a single power law with two free parameters ( $f(\nu) = A(\nu/22 \text{ GHz})^p$ ) as a fitting function; second, we considered a two-component fit, in which one component is given by a power-law, and the other is described by the standard combination of Draine & Lazarian models (CNM, WNM and WIM, with relative amplitudes of 0.43, 0.43 and 0.14, respectively). Finally, we considered a phenomenological approach and tried to fit the data with a single Gaussian law given by  $f(\nu) = A \exp(-(\nu - \nu_0)^2 / (2\sigma^2))$  in order to mimic the behaviour of a general spinning-dust model.

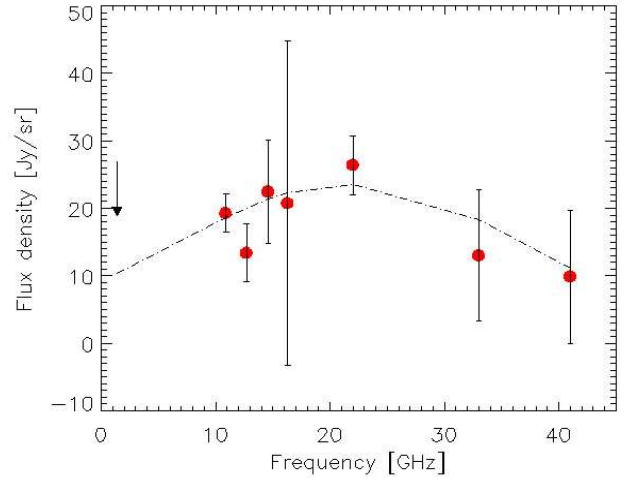


**Figure 17.** Correlation between COSMOSOMAS, WMAP channels and the DIRBE08 map in flux density units (Jy/sr) for  $|b| > 30^\circ$  after masking some localized regions, see text for details. Overplotted is the best fit model of a Gaussian model with parameters  $A = 23.6 \text{ Jy/sr}$ ,  $\nu_0 = 21.7 \text{ GHz}$  and  $\sigma = 15.8 \text{ GHz}$ .

The best fit is obtained in the third case, with a reduced value of  $\chi^2/\text{dof} = 0.72$  (probability of 63%), although the other two cases show similar values for the goodness-of-fit, obtaining 1.05 (39.1%) and 0.93 (46.9%) for model 1 and 2, respectively. We note that in the case of model 1 the index of the power-law ( $p = 0.1 \pm 0.2$ ) rules out synchrotron emission but is compatible with free-free.

For the third model, the best fit parameters (obtained from the marginalized likelihood function) are  $A = 23.5^{+3.9}_{-3.2} \text{ Jy/sr}$ ,  $\nu_0 = 21.7^{+3.8}_{-3.7} \text{ GHz}$  and  $\sigma = 15.8^{+4.0}_{-3.4} \text{ GHz}$ . In Fig. 17 we plot the data of Tab. 10 and this model.

This “blind” best-fit function peaks at a slightly lower frequency than the considered Draine & Lazarian model, and has a slightly broader width. In the case of interpreting this anomalous signal in terms of a spinning dust model, this would have an impact on the actual size distribution of the grains responsible for the emission.

In summary, these results appear to support the existence of a spinning dust microwave emission process at high Galactic latitudes. In order to disentangle whether this anomalous microwave emission is associated to well defined regions as it is the case of the Perseus molecular complex (Watson et al. 2005), or to a diffuse large-scale Galactic component, maps of higher sensitivity and resolution are required in the frequency range 10–30 GHz.

## 5 CONCLUSIONS

We have presented new results of the COSMOSOMAS experiment at 11 GHz for a sky coverage of ca. 6500 sq. deg. A cross-correlation analysis using this new dataset, previous COSMOSOMAS data in the frequency range 12–17 GHz, the 3rd year WMAP data and several foreground templates yields the following results at high Galactic latitude ( $|b| > 30^\circ$ ):

- The presence of a CMB component of amplitude  $27 \pm 2 \mu\text{K}$  in the COSMOSOMAS channels in agreement with the expected

**Table 10.** Temperature correlations between the COSMOSOMAS and WMAP maps and dust maps for different Galactic latitudes. The values are obtained extending the mask to the particular regions where there is a high correlation between COSMOSOMAS and DIRBE08, see text. Errors are  $1\sigma$ .

Template	1420 MHz	C1	C2	C13	C15	C17	WMAP_K	WMAP_Ka	WMAP_Q	WMAP_W
$ b  > 30^\circ$										
A100	$96.1 \pm 571.0$	$4.7 \pm 0.9$	$5.9 \pm 0.8$	$2.4 \pm 0.9$	$2.3 \pm 1.1$	$4.5 \pm 2.7$	$1.9 \pm 0.3$	$0.4 \pm 0.3$	$0.2 \pm 0.2$	$-0.1 \pm 0.2$
DIRBE08	$-139.1 \pm 573.1$	$4.6 \pm 0.9$	$5.8 \pm 0.8$	$2.8 \pm 0.9$	$3.5 \pm 1.2$	$2.5 \pm 2.9$	$1.8 \pm 0.3$	$0.4 \pm 0.3$	$0.2 \pm 0.2$	$-0.2 \pm 0.2$
DIRBE10	$115.0 \pm 568.1$	$4.8 \pm 0.9$	$6.6 \pm 0.8$	$1.2 \pm 0.9$	$-0.6 \pm 1.2$	$2.8 \pm 2.9$	$1.3 \pm 0.3$	$0.3 \pm 0.3$	$0.1 \pm 0.2$	$-0.3 \pm 0.2$
$ b  > 40^\circ$										
A100	$-962.0 \pm 663.1$	$3.5 \pm 1.0$	$3.7 \pm 0.9$	$-0.4 \pm 1.2$	$1.9 \pm 1.5$	$0.6 \pm 3.5$	$1.4 \pm 0.3$	$0.6 \pm 0.3$	$0.3 \pm 0.3$	$0.2 \pm 0.3$
DIRBE08	$-1252.0 \pm 663.0$	$3.4 \pm 1.1$	$3.9 \pm 1.0$	$0.3 \pm 1.2$	$0.8 \pm 1.5$	$-1.2 \pm 3.5$	$1.0 \pm 0.3$	$0.4 \pm 0.3$	$0.2 \pm 0.3$	$0.1 \pm 0.3$
DIRBE10	$-443.1 \pm 659.0$	$3.5 \pm 1.0$	$4.7 \pm 0.9$	$1.1 \pm 1.2$	$-1.4 \pm 1.5$	$-1.0 \pm 3.6$	$0.7 \pm 0.3$	$0.2 \pm 0.3$	$0.1 \pm 0.3$	$-0.1 \pm 0.3$
$ b  > 50^\circ$										
A100	$-1541.0 \pm 733.0$	$1.8 \pm 1.2$	$0.7 \pm 1.1$	$2.5 \pm 1.3$	$3.5 \pm 1.6$	$-2.8 \pm 4.0$	$1.3 \pm 0.3$	$0.5 \pm 0.3$	$0.3 \pm 0.3$	$0.2 \pm 0.3$
DIRBE08	$-1710.0 \pm 732.0$	$0.7 \pm 1.2$	$0.4 \pm 1.1$	$2.5 \pm 1.3$	$2.0 \pm 1.6$	$-4.9 \pm 4.0$	$0.9 \pm 0.3$	$0.4 \pm 0.3$	$0.2 \pm 0.3$	$0.0 \pm 0.3$
DIRBE10	$-656.1 \pm 723.1$	$2.7 \pm 1.1$	$4.3 \pm 1.0$	$3.6 \pm 1.3$	$0.2 \pm 1.6$	$-4.8 \pm 3.9$	$0.8 \pm 0.3$	$0.1 \pm 0.3$	$0.2 \pm 0.3$	$-0.1 \pm 0.3$

CMB fluctuation after removal of the Fourier terms implied in the atmospheric filtering.

- For the angular scales of our experiment, unresolved extragalactic sources are found to be the dominant foreground at 11 GHz. The measured contributions of unresolved radiosources in the range 11–23 GHz are in very good agreement with predictions by de Zotti et al. (2005).

- The synchrotron component at high Galactic latitude is found with an amplitude of 3–6  $\mu\text{K}$  at 11 GHz, and decreases at higher frequency with a temperature spectral index compatible with -3.

- The cross-correlation with the  $\text{H}\alpha$  map gives an amplitude of 3–6  $\mu\text{K}$  at 11 GHz. Correlations with higher frequency COSMOSOMAS and WMAP data verify a temperature spectral index consistent with -2, characteristic of free-free emission.

- A dust correlated emission is detected in each of the COSMOSOMAS channels at  $|b| > 30^\circ$ . The amplitude of the signal ranges from 10–12  $\mu\text{K}$  at 11 GHz down to 4–7  $\mu\text{K}$  in the 12–17 GHz and 2.1–2.8  $\mu\text{K}$  at 22 GHz. The Galactic latitude dependence supports a Galactic origin for this signal. An important fraction of this correlated signal at 11 GHz comes from regions of high dust emission where free-free emission is not well traced by the  $\text{H}\alpha$  template due to extinction. After masking those regions the remaining dust correlated signal detectable in the frequency range 11–33 GHz - of order 5–6  $\mu\text{K}$  at 11 GHz - shows a clear flattening, which is not compatible with the classical spectral index of synchrotron emission. This correlated signal can be described by models resembling spinning dust emission, with an associated flux density peaking around 20 GHz.

## ACKNOWLEDGEMENTS

We are thankful to L. Toffolatti and J. González-Bueno for very useful discussions on unresolved radiosource contributions at the frequencies of COSMOSOMAS. We also thank J.L. Salazar and the personnel of the IAC engineering division, instrument maintenance and operations of Teide Observatory for their support to the COSMOSOMAS experiment. This research has been partially funded by project AYA 2001-1657 and AYA 2005-06453 of the Spanish Ministry of Education and Science.

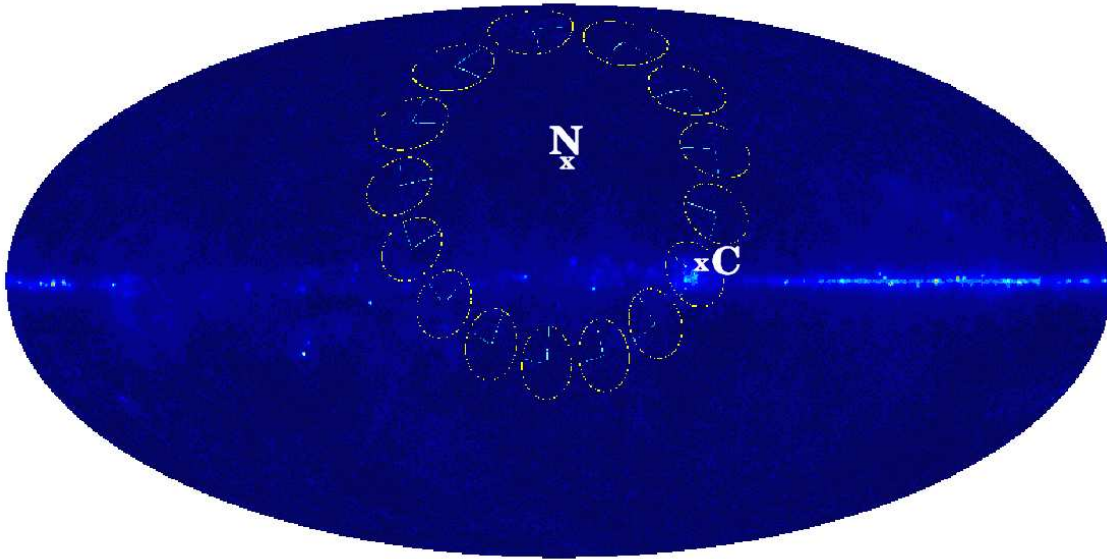


**Figure 18.** COSMO11 scanning strategy together with the two polarization directions observed in Galactic coordinates. The image used for the sky is that provided by WMAP for its lowest frequency channel (K-band, 22.5 GHz), which is the closest to COSMO11 observed frequencies. Top: image centered at Galactic longitude  $0^\circ$ . The Celestial north pole is again marked with an “N”. Cygnus A complex is labelled with a “C”. HEALPix pixelisation scheme is used, (Górski et al. 2005).



## REFERENCES

- Baars, J. W. M., Genzel, R., Pauliny-Toth I. I. K., Witzel, A. 1977, *A&A*, 161, 99
- Battistelli, E.S., Rebolo, R., Rubiño-Martín, J. A. et al. 2006, *ApJ*, 645, L141
- Bennett, C.L., et al., 2003a, *ApJS*, 148, 1
- Bennett, C.L. et al. 2003b, *ApJS*, 148, 97
- Burigana, C., La Porta, L., Reich, P. & Reich, W. 2006, *AN*, 327, 491
- Casassus, S., Cabrera, G. F., Förster, F., Pearson, T. J., Readhead, A. C. S., Dickinson, C. 2006, *ApJ*, 639, 951
- Davies, R. D., Watson, R. A., & Gutiérrez, C. M. 1996 *MNRAS*, 278, 925
- de Oliveira-Costa, A., Kogut, A., Devlin, M.J., Netterfield, C. B., Page L. A., & Wollack, E. J. 1997, *ApJ*, 582, L17
- de Oliveira-Costa, A., Tegmark, M., Page, L.A., & Bouhgn, S. P. 1998, *ApJ*, 509, L9
- de Oliveira-Costa, A. et al. 1999, *ApJ*, 527, L9
- de Oliveira-Costa, A., Tegmark, M., Davies, R. D., Gutiérrez, C. M., Lasenby, A. N., Rebolo, R., & Watson, R. A. 2004, *ApJ*, 606, L89
- de Zotti, G., Ricci, R., Mesa, D., Silva, L., Mazzotta, P., Toffolatti, L., Gonzalez-Nuevo, J. 2005, *A&A*, 431, 893
- Draine, B. T., Lazarian, A. 1998a, *ApJ*, 494, L19
- Draine, B. T., Lazarian, A. 1998b, *ApJ*, 512, 740
- Fernández-Cerezo, S., Gutiérrez, C. M., Rebolo, R., et al. 2006, *MNRAS*, 370, 15-24
- Finkbeiner, D. P., Schlegel, D. J., Frank, C., & Heiles, C. 2002, *ApJ*, 566, 989
- Finkbeiner, D. P. 2003, *ApJS*, 146, 407
- Finkbeiner, D. P., Langston, G.I., & Minter, A.H. 2004, *ApJ*, 617, 350
- Gallegos, J. E., Macías-Pérez, J. F., Gutiérrez, C. M., Rebolo, R., Watson, R. A., Hoyland, R. J., & Fernández-Cerezo, S. 2001, 327, 1178
- Gregory, P. C., Scott, W. K., Douglas, K., Condon, J. J. 1996, *ApJS*, 103, 427
- Górski, K.M., Hivon, E., Banday, A.J., Wandelt, B.D., Hansen, F.K., Reinecke, M., & Bartelmann, M., 2005, *ApJ*, 622, 759-771.
- Gutiérrez, C. M., Rebolo, R., Watson, R. A., Davies, R. D., Jones, A. W., & Lasenby, A. N. 2000, *ApJ*, 529, 47
- Haslam, C. G. T., Stoffel, H., Salter, C. J., Wilson, W. E. 1982, *A&ASS*, 47, 1
- Hancock, S., Gutiérrez, C. M., Davies, R. D., Lasenby, A. N., Rocha, G., Rebolo, R., Watson, R. A., & Tegmark, M. 1997, *MNRAS*, 289, 505
- Hinshaw, G., Nolta, M. R., Bennett, C. L., Bean, R. et al. [astro-ph/0603451](https://arxiv.org/abs/astro-ph/0603451). To be published.
- Kogut, A., Banday, Bennett, C. L., Gorski, K. M., Hinshaw, G., & Reich, W. T., *ApJ*, 1996, 460, 1
- Kühr, H., Witzel, A., Pauliny-Toth, I. I. K., Nauber, U. 1981, *A&A*, 45, 367
- Leitch, E. M., Readhead, A. C. S., Pearson, T. J., & Myers, S. T. 1997, *ApJ*, 486, L23
- Mason, B. S.; Pearson, T. J.; Readhead, A. C. S.; Shepherd, M.; Sievers, J.; Udomprasert, P.; Cartwright, J. K.; Padin, S. 2001. 20th Texas Symposium on relativistic astrophysics, Austin, Texas, 10-15 December 2000, Melville, NY: American Institute of Physics, 2001, xix, 938 p. AIP conference proceedings, Vol. 586. Edited by J. Craig Wheeler and Hugo Martel.
- Reich, P. & Reich, W. 1986, *A&ASS* 163, 205
- Schlegel, D.J., Finkbeiner, D.P., & Davis, M. 1998, *ApJ*, 500, 525
- Watson, R.A., Rebolo, R., Rubiño-Martín, J.A., Hildebrandt, S.R., Gutiérrez, C.M., Hoyland, R.J., & Battistelli, E.S. 2005. *ApJ*, 624, L89
- Wollleben, M., Landecker, T. L., Reich, W., & Wielebinski, R. 2006, *A&A*, 448, 411